

Open Wireless Digital Twin: End-to-End 5G Mobility Emulation in O-RAN Framework

TETSUYA IYE¹, MASAYA SAKAMOTO², SHOHEI TAKAYA¹, EISAKU SATO¹,
YUKI SUSUKIDA¹, YU NAGAOKA³, KAZUKI MARUTA⁴ (Senior Member, IEEE),
AND JIN NAKAZATO⁵ (Member, IEEE)

¹Kozo Keikaku Engineering Inc., Tokyo, Japan

²Independent Researcher

³Department of Electronics and Computer Systems, Graduate School of Engineering, Takushoku University, Tokyo, Japan

⁴Department of Electrical Engineering, Graduate School of Engineering, Tokyo University of Science, Tokyo, Japan

⁵Graduate School of Information Science and Technology, The University of Tokyo, Tokyo, Japan

CORRESPONDING AUTHOR: Tetsuya Iye (e-mail: tetsuya-ye@kke.co.jp).

This research and development work was supported in part by Fundamental Technologies for Sustainable Efficient Radio Wave Use R&D Project (FORWARD) from the Ministry of Internal Affairs and Communication (receipt number JPMI240310001), Japan.

ABSTRACT This paper presents an end-to-end wireless digital twin platform constructed using open-source software and open data to enhance the evaluation of mobile communication systems. The proposed open wireless digital twin (OWDT) integrates OpenAirInterface (OAI) for 5G NR protocol stack emulation and NVIDIA Sionna RT for high-resolution ray tracing based radio propagation modeling. This integration enables realistic emulation of vehicular mobility scenarios, leveraging real-world geographic and building data to bridge the gap between theoretical simulations and real-world deployments. The platform utilizes O-RAN's Near-RT RIC via OAI FlexRIC to dynamically monitor key performance indicators (KPIs) such as RSRP, MCS, BLER, and throughput in real time. Through extensive evaluation in urban environments, this study demonstrates the validity of the emulation framework, revealing its capability to replicate real-world communication dynamics with high fidelity. The results underscore the potential of OWDT in accelerating wireless system development, reducing experimental costs, and optimizing network configurations.

INDEX TERMS Digital twin, Emulation, Mobility, 5G NR, O-RAN, OpenAirInterface, Sionna RT, SUMO, PLATEAU, OpenStreetMap.

I. INTRODUCTION

IN the research and development of wireless-assisted connected autonomous vehicles (CAVs) for future intelligent transportation systems (ITS), it is necessary to measure and evaluate changes in various mobile communication key performance indicators (KPIs) as vehicle-mounted antennas move [1], [2]. However, challenges arise due to the difficulty in ensuring the reproducibility of measurement data caused by the complex radio propagation characteristics of real-world physical environments. In addition, the complexity of standard specifications for mobile communications, such as 5G NR, poses challenges in interpreting and evaluating the obtained data. To address these challenges, emulation technology, which allows experiments to be conducted under

ideal conditions using primarily real equipment, is beginning to gain attention as a preliminary step before conducting experiments in increasingly complex field environments.

It is common for next-generation wireless communication systems (e.g., 6G) to go through research, development, and demonstration stages before being deployed in society. In particular, it is important to evaluate the performance of a newly developed system through demonstration experiments based on actual usage scenarios. At the same time, the demonstration itself is a significant technical challenge in the research and development of wireless technologies for societal deployment, often referred to as one of the 'valleys of death.' Challenges associated with implementation and evaluation include: (1) The differences between simulation

models and real equipment, such as RF front-ends. (2) Demonstration experiments require not only infrastructure costs and preparation time but, in some cases, the acquisition of radio station licenses, resulting in significant time and financial constraints that limit the ability to repeat comparative evaluations. (3) The increasing complexity of wireless communication system protocols as they become more advanced. (4) The difficulty of accurately simulating the radio propagation environment when pre-evaluating actual demonstration scenarios.

Against this backdrop, solutions addressing challenges (1) and (2) have led to growing demand beyond the wireless communication field for conducting scenario testing in virtual environments of digital twins that replicate the real world with high fidelity before conducting field experiments [3], [4]. In fact, the development of digital twin platforms for wireless communications has been increasing [5]–[14]. The key technical aspects of realizing a digital twin include emulation technology, which ensures high fidelity and real-time responsiveness in the virtual space, as well as consistency with measurement data that links the virtual and real worlds. In wireless digital twins, these features enable the verification of newly proposed methods before demonstration experiments, reproducibility of time-varying KPIs that are difficult to achieve in real-world communication systems, and optimization of deployment parameters. Thus, the development of digital twin platforms and emulation-based validation is emerging as a promising methodology for bridging the technological gap between theoretical development, simulations, and demonstration experiments; accelerating the cycle that connects research innovations to societal deployment.

Regarding the challenge of (3), recent trends in wireless communication research and development show significant advancements in the development of various open-source software (OSS) and the use of open data. One of the key factors behind this global open innovation trend is the increasing sophistication, diversification, and complication of wireless communication technologies that prevent a single company or organization from conducting full-stack research and development independently. Many commercial wireless communication technologies are standardized by organizations, meaning that common global specifications are defined. As a result, implementing these common specifications as OSS by engineers worldwide, regardless of any specific for-profit organization, is an economically rational approach on a global scale. From a user perspective, OSS allows the low-cost construction of research and development environments while also enabling flexible customizations that are difficult to achieve with commercial software. 5G NR, which is being standardized under 3GPP, is no exception. As shown in Table 1, OSS implementations have emerged to perform functions related to the 5G Radio Access Network (RAN), the 5G Core Network (CN), the User Equipment (UE), and the O-RAN [15]–[24]. Among them, OpenAirInterface

TABLE 1. Comparison between current 5G/O-RAN OSS and this study.

Software/Community	CN	RAN	UE	OTA	Prop.	O-RAN
OAI (EURECOM) [15]	✓	✓	✓	✓	-	✓
free5GC (free5GC.org) [16]	✓	-	-	-	-	-
Open5GS (Individual) [17]	✓	-	-	-	-	-
Magma (MCF) [18]	✓	✓	-	-	-	-
AETHER (ONF) [19]	✓	✓	-	-	-	✓
srsRAN (SRS) [20]	-	✓	✓	✓	-	-
UERANSIM (Individual) [21]	-	✓	✓	-	-	-
Sionna (NVIDIA) [22]	-	✓	-	-	✓	-
dRAX (Accelleran) [23]	-	✓	-	✓	-	✓
O-RAN SC (OSC) [24]	-	-	-	-	-	✓
This Study	✓	✓	✓	✓	✓	✓

(OAI) [15] stands out as a widely used OSS in research and development, offering detailed implementations across 4G LTE/5G NR CN, RAN, UE, and O-RAN, along with support for Over-the-Air (OTA) experiments involving SDR devices. While many OSS projects focus on signal processing and information processing above the lower layers of wireless devices, NVIDIA Sionna provides physical layer signal processing capabilities. In addition, Sionna RT [25] offers GPU-accelerated differentiable ray tracing for radio propagation simulations, further expanding its applicability in wireless research.

The modeling of radio propagation, which falls under difficulty (4), has been studied for improved accuracy using both stochastic and deterministic approaches. The stochastic approach allows for the construction of channel models that statistically approximate experimental measurement results by parameter fitting. On the other hand, when 3D building models and terrain data are available, deterministic approaches such as ray tracing can explicitly track propagation paths and perform high-fidelity channel calculations from a microscopic perspective. In particular, ray tracing excels at simulating delay profiles in environments with significant multipath propagation. While multipath signals are treated as fading effects at the receiver, there exists a trade-off between the number of delay taps of signals and the computational processing cost. Real-time processing is essential to ensuring the emulation functionality of digital twins. Therefore, efficient computation mechanisms that maintain the necessary number of delay taps to reproduce realistic fading effects while ensuring real-time calculation of received signals is necessary. This study focuses on performing real-time convolution processing on baseband signals using precomputed time-evolving radio propagation information in a CPU-only environment.

Based on the above background, this study proposes the integration of OAI and Sionna RT to construct an OSS based end-to-end (E2E) open wireless digital twin (OWDT) platform. Here, E2E refers to the communication section from the core network (CN), through the radio access network (RAN), including the base station (gNB), to UE.

Specifically, we perform wireless communication emulation that considers realistic propagation environments based on site-specific mobility scenarios using actual building shapes and geographic data while utilizing O-RAN functionalities to monitor KPIs in real time. In general, digital twin based communication involves replicating real-world communication environments within a virtual space [6], [8], [11]. This replica includes 3D building structures, material properties, and detailed information on gNBs and UE antennas, such as their positions, orientations, and movements. The higher the accuracy of this information, the more precisely the emulation can capture real wireless communications. Recently, a full-stack simulation environment that integrates open-source network simulator ns-3 and Sionna RT, considering deterministic channel models, has been reported [14]. In the commercial sector, companies like Ericsson have introduced network digital twin (NDT) solutions, incorporating proprietary AI technologies [26]. Our research takes a further step into the boundary domain between the physical layer in wireless communication systems and radio propagation, directly incorporating the effects of multipath fading on IQ sample-level baseband signals. To the best of our knowledge, this study represents the first case of real-time E2E emulation on a commercial off-the-shelf (COTS) CPU based computing server that does not abstract the L1 layer processing of the OSI reference model while considering multipath radio propagations. Our study only considers the effects of frequency-selective fading caused by the relative position updates of the transmitter and receiver in each snapshot of the mobility scenario without considering the effects of the velocity of the vehicle and the Doppler shift.

This paper is structured as follows. Section II introduces the E2E system architecture of OWDT, incorporating the 5G NR protocol stack implemented by OAI, the Near-realtime RAN intelligent controller (Near-RT RIC) enabling O-RAN-compliant key performance measurement (KPM), and the propagation channels generated by Sionna RT. It also describes the hardware environment in which these components were deployed. Next, the workflow for executing mobility emulation scenarios, such as vehicular driving, within the OWDT platform is explained. This section also introduces the OSSs and open data utilized in the workflow. Furthermore, it provides a detailed discussion of the convolution method used to apply channel impulse responses to the baseband signals, which serves as the integration point between OAI and Sionna RT. Section III evaluates the data obtained through ray tracing and the KPIs measured from OAI after applying this data to the system while executing mobility scenarios on the platform. Finally, Section IV concludes the paper with a discussion of future perspectives.

II. METHODS
A. SYSTEM ARCHITECTURE

We realized OWDT by integrating OAI, which reproduces the 5G NR protocol stack from the PHY layer and above,

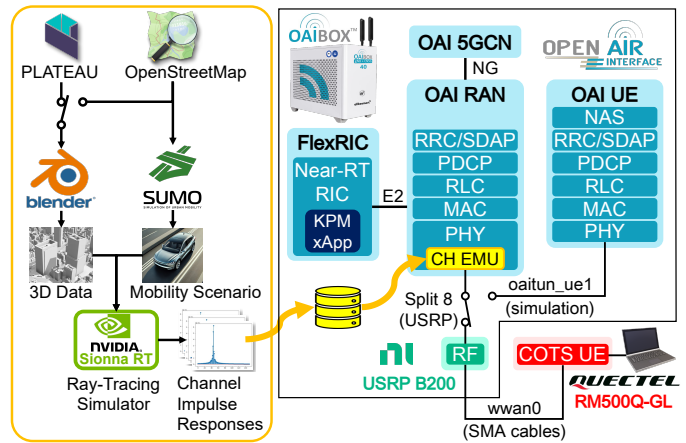


FIGURE 1. Workflow of generating channel impulse responses for mobility scenario (left panel) and 5G NR system architecture including 5GCN, RAN, Near-RT RIC, and UE developed by the OAI project, along with the RF device serving as the RU and COTS UE. (right panel).

with NVIDIA Sionna RT, which enables the construction of a deterministic channel model through ray tracing. In this environment, channel impulse responses (CIRs) pre-generated using Sionna RT are applied as propagation channels between the gNB and UE in OAI. This allows us to simulate a scenario where the UE moves within a 3D map while performing 5G communication, even though the gNB and UE remain physically connected over the cable. Furthermore, we can observe how KPIs, such as reference signal received powers (RSRPs), modulation and coding schemes (MCSs), block error rates (BLERs), and throughputs, dynamically change in real time during the scenario. These measurements are performed by O-RAN standard KPM v3.00 [27], one of the service models supported by FlexRIC [28], a near-RT RIC that provides an xApp SDK framework developed within OAI.

The fundamental architecture of OWDT is illustrated on the right side of Fig. 1. The hardware components that constitute the architecture are as follows: (i) A COTS server to implement 5GCN, gNB, and Near-RT RIC, along with a software-defined radio (SDR) device responsible for RF signal processing. The server is equipped with an AMD Ryzen 9 7900X 12-core processor (x24), 32 GiB RAM, and runs Ubuntu 22.04.4 LTS with Linux kernel version 6.8.1-060801-generic. The NI USRP B200 is used as an SDR device, connected via USB. In practice, this setup is realized using Allbesmart’s OAIBOX™ 40. (ii) A computation server used for ray tracing based radio propagation simulation with Sionna RT. The server is equipped with an Intel(R) Xeon(R) Silver 4310 @ 2.10 GHz CPU, 256 GiB RAM, an NVIDIA A100 GPU (80 GB), and runs Ubuntu 22.04.4 LTS. (iii) A COTS laptop and SDR device pair for implementing an NR UE, or alternatively, any UE module that can be physically connected to the gNB via an RF cable. In this work, the Quectel RM500Q-GL UE module is connected to the laptop with an 11th Gen Intel Core i7-11370H @ 3.30 GHz (x8), 15.4 GiB RAM, and Ubuntu 20.04 LTS via USB.

B. WORKFLOW

In this study, an E2E wireless emulation following the mobility scenario is performed in OWDT through the following five steps: 1) Preparation of 3D building data, 2) Generation of mobility scenarios, 3) Calculation of radio propagation via ray tracing, 4) Convolution of channel impulse response, and 5) Wireless emulation using OAI. First, an overview of each step is provided, followed by an explanation of the specific models and parameters adopted in this study.

1) Preparation of 3D Building Data

To achieve higher resolution in radio propagation simulations, it is essential to prepare highly detailed 3D building data in terms of size and location and perform site-specific deterministic evaluations. The 3D urban data provided by the PLATEAU, an open data project promoted by the Ministry of Land, Infrastructure, Transport, and Tourism (MLIT) in Japan [29], adopts building height measurements obtained via aerial surveying and generally provides higher accuracy in the height dimension compared to OpenStreetMap (OSM) [30]. This data is available in CityGML format, which cannot be directly handled by Sionna RT in this study. Therefore, the open-source 3D CG software Blender 4.2 [31] is used to convert it into PLY format. If OpenStreetMap is used as 3D building data, it can be imported into Blender using Blossm [32]. To assign materials to the polygon surfaces of the imported 3D model, the Mitsuba Blender Add-on [33] is used. In this study, two scenario areas are evaluated in Tokyo, Japan: Shin-nakano station and Shibuya station surroundings. The 3D model of the Shin-nakano station area is provided at Level of Details 1 (LOD1), where buildings are represented as solids, and all surfaces covering the solid are described as polygon elements. On the other hand, the 3D model of the Shibuya station area is provided at LOD2, which allows for more detailed structures than LOD1, enabling the representation of walls, roofs, and floors with different materials. For the LOD1 Shin-nakano model, all materials, including roads, walls, and roofs, are designated as concrete, and the scene file is saved in XML format. In contrast, in the LOD2 Shibuya model, glass is assigned to building walls, concrete to road surfaces, and metal to overpass surfaces. These materials are determined using the values of the real part of relative permittivity and conductivity, given by the equations $\epsilon_r = a(f \cdot 10^{-9})^b$, $\sigma_c = c(f \cdot 10^{-9})^d$, where f is the carrier frequency, as described in [34]. The specific parameter values for each material and the values of ϵ_r and σ_c at the frequency used in this study are shown in Table 2.

2) Generation of Mobility Scenarios

The generation of mobility evaluation scenarios is handled by SUMO (Simulation of Urban MObility) [35]. SUMO is a traffic simulator capable of realistically replicating

TABLE 2. Material properties for ray-trace simulation [34].

Material class	Real part of relative permittivity		Conductivity [S/m]		ϵ_r	σ_c (4.01916 GHz)
	a	b	c	d		
Vacuum	1	0	0	0	1	0
Concrete	5.24	0	0.0462	0.7822	5.24	0.1372
Glass	6.31	0	0.0036	1.3394	6.31	0.0232
Metal	1	0	10^7	0	1	10^7

vehicle movement by incorporating traffic lights, multiple lanes, speed limits for each road, gradual acceleration and deceleration, and interactions with other vehicles. Based on OpenStreetMap road data, SUMO enables the creation of vehicle mobility scenarios by specifying the driving lanes and their sequence, generating time-series updates of vehicle position coordinates (x, y) . Although not used in this study, the mobility scenario can also include the velocity vector of the vehicle at each snapshot, which can be utilized to compute Doppler shift as a key factor affecting fast fading. In both the Shin-nakano and Shibuya scenarios, vehicles temporarily stop at traffic lights at intersections and make left turns. Additionally, in the narrow residential streets of Shin-nakano, where intersections and T-junctions lack traffic lights, vehicles either slow down or make a temporary stop before proceeding straight or making a left turn.

3) Channel Impulse Response Calculation Using ray tracing

Using any ray tracing simulator, a deterministic and site-specific channel model for mobility can be computed by integrating the mobility scenario generated by SUMO with the 3D urban geometry data from OSM or PLATEAU. At arbitrary time intervals, the CIR can be calculated by considering reflections, diffractions, and diffuse scatterings between the gNB, which is fixed at a specific location, and the UE, which moves according to the mobility scenario. However, to enable real-time KPI measurement using only commercial CPUs, Doppler shift caused by the velocity of the moving object is not considered, and only static multipath fading is evaluated at each snapshot.

NVIDIA Sionna RT [25] is an OSS that leverages GPU acceleration based on TensorFlow to perform fast ray tracing simulations of propagation environments. Sionna RT was used in this study to efficiently conduct ray tracing over hundreds of snapshots throughout the scenario. However, other ray tracing simulators that can output CIR, such as Wireless InSite [36] and Opal [37], can also be applied to the same scenario [36]–[40]. The resolution of the CIR output from the simulation depends on the 3D model and the mobility scenario. In particular, in complex urban environments, achieving a high-fidelity digital twin is only feasible with high-quality spatiotemporal data.

The simulation parameters for ray tracing are listed in Table 3. The common parameters for both radio propagation and system model include frequency band, center frequency,

TABLE 3. System parameters for Sionna RT and OAI.

Simulation	Parameter	Value (Units)	
Common	Frequency band	n77	
	Carrier frequency f	4.01916 GHz	
	Number of transmitters M_T	1	
	Number of receivers M_R	1	
	Number of transmit antenna N_T	1	
	Number of receive antenna N_R	1	
	Sampling rate f_{samp}	46.08 Msps	
	Sionna RT	Antenna pattern $g(\theta, \phi)$	1 (0 dBi: isotropic)
UE antenna height		1.5 m	
gNB antenna height		22.0 m (Shin-nakano) 10.5 m (Shibuya)	
Reflection		True	
Diffuse Scattering		False	
Max depth		5	
Diffraction		True	
Number of rays		10^7	
Coverage map resolution		1 m \times 1 m	
Coverage map height		1.5 m	
Scenario interval t_{int}		100 ms	
Number of snapshots		570 (Shin-nakano) 230 (Shibuya)	
OAI		Technology	5G NR SA
		Channel bandwidth BW	40 MHz
	Subcarrier spacing	30 kHz	
	FFT size	1536	
	Antenna	SISO	
	Duplex mode	TDD	
	TDD slot pattern	DDDSU	
	Special slot format	6D+4G+4U	

the number of transceivers, the number of antennas per transceiver, and sampling rate. In this study, we adopt n77 band (3.3 GHz–4.2 GHz), with a center frequency of 4.01916 GHz. The number of transceivers and the number of antennas per transceiver are set to one, meaning a single-input single-output (SISO) communication model is considered between the gNB and UE. The sampling rate is set to $f_{\text{samp}} = 46.08$ Msps, as supported by the USRP B200 used on the gNB side. This sampling rate is also provided as an input argument to Sionna RT functions when bandwidth limitation is applied to the delay profile.

For ray tracing simulation, an isotropic antenna pattern is assumed, with $g(\theta, \phi) = 1$, i.e., 0 dBi for all directions. Reflection is enabled by setting `True`, and the maximum number of reflections is set to five by defining `max_depth = 5`. When diffraction is set to `True`, the model considers up to one diffraction per path without reflections. In other words, the combination of reflections and diffractions is not calculated. In Sionna RT, diffuse scattering models the interaction of electromagnetic waves with rough surfaces, causing energy to be scattered in multiple directions rather than following a single specular reflection path. The

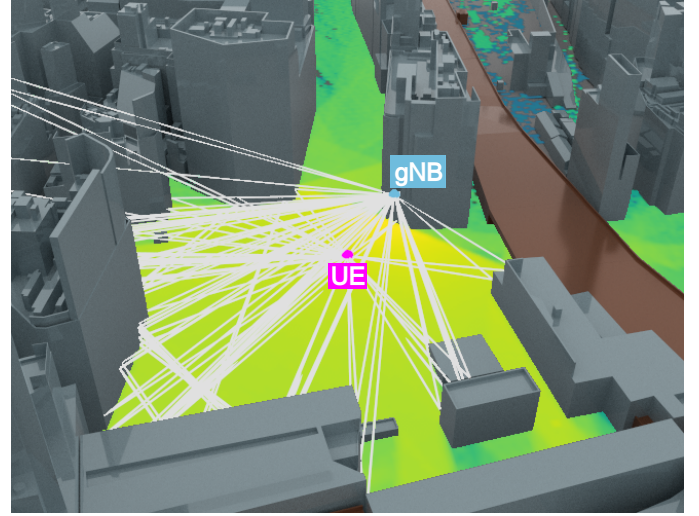


FIGURE 2. Ray tracing simulation for Shibuya scenario.

scattering is tested under four different conditions: `False`, `True` with scattering keep probability values of 10^{-6} , 10^{-5} , and $5 \cdot 10^{-5}$, up to the upper limit of GPU memory constraints. The resulting path gain differences were at most 0.12 dB, with an absolute mean difference of 0.002 dB throughout the Shin-nakano scenario. Given this minimal impact, the CIR used in this study is derived from the simulation with diffuse scattering disabled by setting `False`.

For ray tracing, the shoot-and-bounce approach with the “fibonacci” path search method [25] was used, setting the number of candidate traced rays to 10^7 . The gNB–UE link’s complex amplitude and delay were computed for each snapshot by updating the UE’s coordinates every 100 ms according to the mobility scenario. For the Shin-nakano scenario, 570 snapshots were obtained over 57.0 s, while the Shibuya scenario involved 230 snapshots over 23.0 s. The total computation time for ray tracing across all snapshots was 13.5 s for Shin-nakano and 8.9 s for Shibuya. One of the snapshots from the Shibuya scenario is shown in Fig. 2.

A radio propagation channel model is used to generate a delay profile, i.e., complex amplitude $a_p \in \mathbb{C}$ and delay $\tau_p \in \mathbb{R}$ for each link between the transmitter antenna and receiver antenna for p^{th} -path among $P \in \mathbb{N}$ paths. The amplitudes and delays are assumed to be time-independent. Such a delay profile against the delay time τ corresponds to be

$$h(\tau) = \sum_{p=0}^{P-1} a_p \delta(\tau - \tau_p), \quad (1)$$

where $\delta(\cdot)$ is the Dirac delta measure. The resulting discrete-time CIR under bandwidth limitation assuming a sinc filter for pulse shaping and receiving filtering is computed as follows:

$$\bar{h}[k] = \sum_{p=0}^{P-1} a_p \text{sinc}(k - f_{\text{samp}}\tau_p), \quad (2)$$

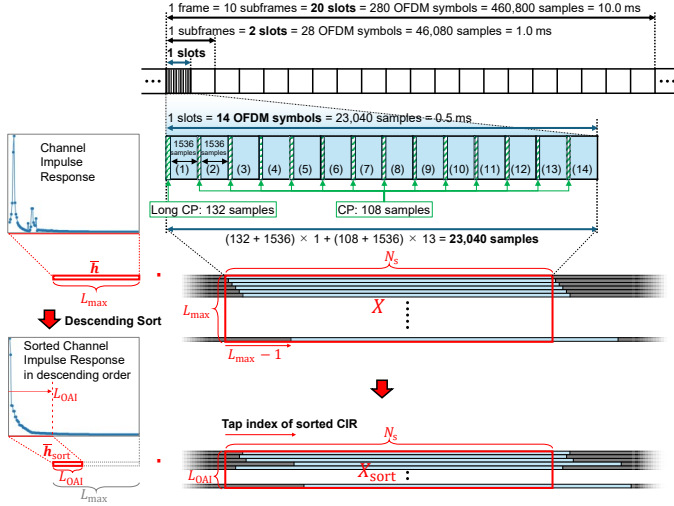


FIGURE 3. Implementation of CIR convolution for the proposed OWDT in OAI.

where $k \in \mathbb{Z}$ is the delay index corresponding to the sampling interval $1/f_{\text{samp}}$. Since the ideal sinc filter violates causality and is non-time-limited, it is necessary to consider from $k = -\infty$ to $k = +\infty$. However, in practice, these lower and upper limits need to be set to reasonable finite values, which can be computed using the Sionna RT `time_lag_discrete_time_channel()` function from a given sampling rate and sufficiently reasonable maximum delay spread $3 \mu\text{s}$ to be $k = -6$ and $k = L_{\text{max}} - 1 = 145$. Here, for simplicity, we set the lower limit of the considered delay index to $k = 0$.

4) Convolution of Channel Impulse Response

In OAI software, wireless emulation can be executed by convolving the precomputed CIR with the baseband signal in real time according to the time progression of the mobility scenario, thereby reflecting the propagation environment in the transmitted and received signals. This process allows the time evolution of the channel due to changes in the position of the moving object to be reflected in the KPIs obtainable from OAI.

In the OAI source code, baseband IQ samples corresponding to the lowest part of PHY layer are handled within the `tx_rf()` and `rx_rf()` functions in the `nr-ru.c` file. The 5G NR frame format at the baseband IQ sample level and the CIR convolution method are illustrated in Fig. 3. In OAI RAN, the time-domain signal is stored in every slot as `txData` and `rxData`, where the baseband signal of CP-OFDM is represented as $N_s (= \text{FFT size} \times 15)$ complex IQ sample data. To incorporate the delay tap effects of a CIR snapshot into the baseband signal, a matrix $X \in \mathbb{C}^{L_{\text{max}} \times N_s}$ is generated by shifting the baseband signal sample-by-sample for the total number of CIR taps $L_{\text{max}} (= 146)$. Applying the complex CIR vector $\bar{\mathbf{h}} \in \mathbb{C}^{L_{\text{max}}}$ from the left and computing the inner product results in the received

signal $\mathbf{y} \in \mathbb{C}^{N_s}$ with multipath delay components. However, in our environment, even with the use of a high-performance computation library ‘BLIS’ (described later), real-time convolution of the L_{max} -tap delay components obtained from ray tracing was not feasible.

Therefore, considering the most significant contributions first, the CIR $\bar{\mathbf{h}}$ was sorted in descending order as $\bar{\mathbf{h}}_{\text{sort}} \in \mathbb{C}^{L_{\text{OAI}}}$, and the rows of the baseband delay matrix X were reordered accordingly to form $X_{\text{sort}} \in \mathbb{C}^{L_{\text{OAI}} \times N_s}$. Here, the number of leading taps to be read was parameterized as L_{OAI} to determine a real-time executable upper limit. This approach allows the computation to reflect the most significant multipath components first. The convolution operation was implemented within the `rx_rf()` and `tx_rf()` functions on the OAI gNB using `cblas_cgemm` from the high-performance matrix computation library ‘BLIS’ [41]. Specifically, convolution was applied to the baseband signal before cable transmission from the gNB for downlink (DL) and after cable reception from the UE for uplink (UL). The function `cblas_cgemm` multiplies two complex matrices AB and multiplies the resulting matrix by a complex constant α . It then multiplies matrix C by another complex constant β . It stores the sum of these two products in matrix C as follows: $C \leftarrow \alpha AB + \beta C$. In our study, we use this function to perform the following calculations:

$$\mathbf{y} = s\bar{\mathbf{h}}X + \sigma\mathbf{w} \approx s\bar{\mathbf{h}}_{\text{sort}}X_{\text{sort}} + \sigma\mathbf{w}, \quad (3)$$

where $s \in \mathbb{R}$ is the signal amplitude gain, $\sigma \in \mathbb{R}$ is the noise amplitude gain, and $\mathbf{w} \in \mathbb{C}^{N_s}$ is the normalized complex Gaussian noise. To examine this equation in more detail, we express it at the sample time level as follows.

$$y[n] = \sum_{k=0}^{L_{\text{OAI}}-1} s\bar{h}[k]x_k[n-k] + \sigma w[n], \quad (4)$$

where $n \in \mathbb{Z}$ denotes the index for the sampling time.

In general, in a time-invariant multipath delay environment, channel reciprocity is valid due to the absence of Doppler spread [42]. Thus, in this mobility scenario, the theoretical validity of overlaying the same CIR on both DL and UL in the OAI gNB is ensured.

To more finely reproduce the effects of CIR on the transmitted and received signals, it would ideally be necessary to perform convolution with a time-varying CIR for each IQ sample, considering the Doppler shift. However, from a computational cost perspective, real-time execution is infeasible without hardware acceleration such as FPGA or GPU [43]. In this study, to achieve real-time E2E wireless emulation on a commercial CPU-equipped server and a commercial SDR without using such accelerators, convolution with a time-invariant CIR is performed every 100 ms. As mentioned earlier, signal processing in OAI operates on a slot basis, meaning that with the current parameter settings, CIR convolution is performed once every 0.5 ms. That is, the CIR data is updated every 200 iterations.

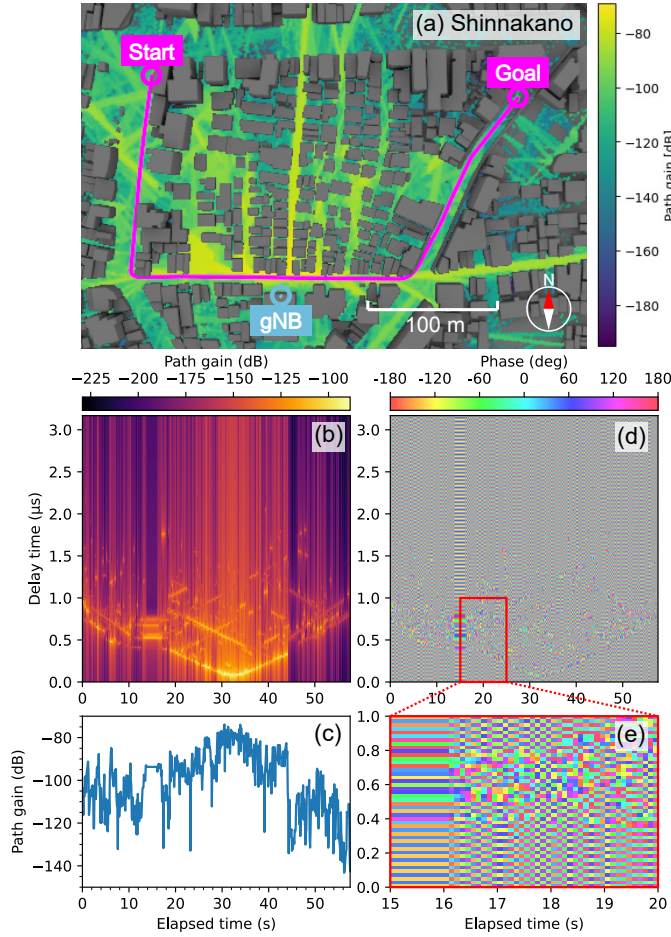


FIGURE 4. (a) Vehicle route on path gain coverage map for Shin-nakano scenario, (b) Power delay profile, (c) path gain, (d) phase delay profile, and (e) enlarged view of (d) for Shin-nakano scenario.

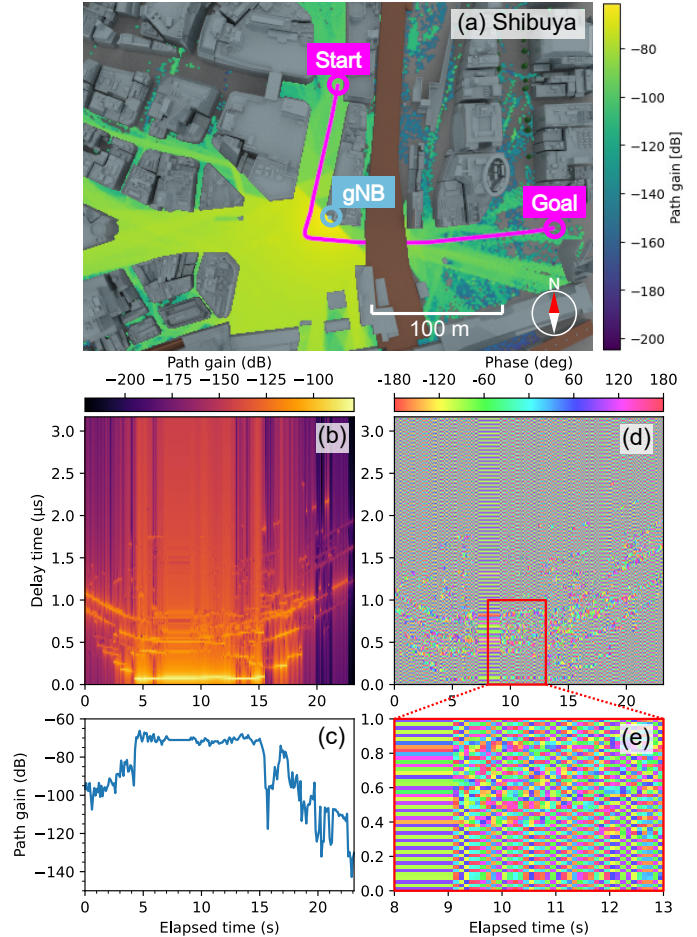


FIGURE 5. (a) Vehicle route on path gain coverage map for Shibuya scenario, (b) Power delay profile, (c) path gain, (d) phase delay profile, and (e) enlarged view of (d) for Shibuya scenario.

5) Wireless Communication Emulation Using OAI

The system parameters configured in OAI are summarized in the lower part of Table 3. The bandwidth BW is set to 40 MHz, which is the maximum achievable bandwidth within the constraints of the sampling rate. The subcarrier spacing is set to 30 kHz, corresponding to numerology $\mu = 1$. The sampling rate and corresponding FFT size are 1,536 points. Since only one TX and one RX antenna are used, the system operates in a SISO configuration. The duplex mode is TDD, and the slot pattern follows ‘DDDSU’. The special slot format follows a typical pattern with 6 DL symbols, 4 guard symbols, and 4 UL symbols.

III. RESULTS AND DISCUSSION

A. RAY TRACING SIMULATION RESULTS

Fig. 4(a) and Fig. 5(a) show bird’s-eye views of the 3D models of Shin-nakano and Shibuya, depicting the fixed gNB position and the vehicle’s movement trajectory overlaid with a path gain heatmap, respectively. The heatmaps are drawn on the horizontal planes at $z = 1.5$ [m], matching the height of the moving UE. The paths considered in the path

gain coverage map, and CIR calculation include the line-of-sight (LoS) path, diffraction paths with up to one diffraction event, and specular reflections up to the number of reflections specified by max_depth .

In the Shin-nakano scenario, the radio propagation environment is complex due to the presence of residential and low-rise buildings and narrow streets. Additionally, the 3D model provided by PLATEAU for the Shin-nakano area is at Level of Detail 1 (LOD1), resulting in relatively simple building shapes. In this mobility scenario, the vehicle starts moving from a location far from the gNB at $t = 0$ and stops briefly at a traffic light between $t = 13.8$ and $t = 16.0$. Upon the green light, it makes a left turn and enters the street in front of the building where the gNB is installed. The vehicle continues eastward, passing in front of the gNB, then briefly stops at another intersection before making another left turn. It then proceeds into a shopping street, heading north-northeast. This scenario consists of 570 snapshots, corresponding to 57.0 s of mobility data. Using the CIR obtained every 100 ms, the power delay profile (PDP), calculated as the square of the complex amplitude, is shown

in Fig. 4(b), and the phase delay profile is shown in Fig. 4(d). Around $t = 18$ [s], as the vehicle enters the street in front of the gNB, the LoS path component appears. As the vehicle approaches the gNB, the signal strength increases, and the delay decreases. When the vehicle passes the gNB and moves away, the signal strength weakens, the delay increases, and the LoS component exhibits a V-shaped pattern on the PDP. After the second left turn, not only does the LoS component diminish, but the number of reflection paths also drops significantly, resulting in approximately 30 dB of path gain attenuation. The change in the total path gain, obtained by summing all complex amplitudes in the CIR, is shown in Fig. 4(c). The results clearly show the plateau period during the stop, the maximum value around $t = 32$ [s], and a sharp 30 dB drop around $t = 44$ [s]. Next, we discuss the phase behavior shown in Figs. 4(d) and (e). Fig. 4(d) indicates rapid phase fluctuations for each tap along the vertical delay time axis. Examining the magnified view in Fig. 4(e), the phase remains constant during the stop, then starts fluctuating once the vehicle begins moving. Along the LoS path trajectory observed in the PDP, the phase exhibits a consistent trend. However, it should be noted that this study does not account for time variations within the 100 ms intervals, and as a result, the phase values show discontinuous transitions in each snapshot. This indicates that our study does not take into account the Doppler effect.

The Shibuya scenario, as shown in Fig. 5(a), involves a route where the vehicle turns left in front of the gNB antenna installed at the corner of an intersection, passes under a brown-colored overpass, and moves away from the gNB. Differences from the Shin-nakano scenario include wider roads and building facades set as glass surfaces, representing an urban business district. In the mobility scenario, the vehicle starts moving from the north and stops briefly at the scramble intersection due to a traffic signal between $t = 7.2$ [s] and $t = 9.1$ [s]. When the light turns green, the vehicle begins a left turn and continues eastward in a straight line. The PDP obtained from the CIR is shown in Fig. 5(b), and the phase delay profile is shown in Fig. 5(d). Around $t = 4.2$ [s], as the vehicle enters the gNB's LoS range, the path gain sharply increases and maintains a plateau until approximately $t = 15.4$ [s], when the LoS component disappears due to the building shadow, causing a sudden drop in path gain. The bright stepped lines visible in the PDP before and after the LoS interval represent first-order and second-order reflections, while higher-order reflections are visible only before the plateau. Examining the magnified view in Fig. 5(e), similar to the Shin-nakano scenario, the phase remains stable during the stop and begins to fluctuate as the vehicle starts to move.

B. OAI KPM RESULTS

By installing and running FlexRIC, which functions as an O-RAN-compliant Near-RT RIC, various KPIs can be obtained in compliance with the E2 Service Model (E2SM) KPM

TABLE 4. DL/UL KPI results from OAI for the baseline measurement.

KPI	Value (Units)
RSRP	-63 dBm
DL MCS	27
DL BLER	$2.62 \cdot 10^{-5}$
DL Throughput	150.14 Mbps
UL MCS	15.21
UL BLER	0.0963
UL Throughput	26.29 Mbps

v03.00. In this study, we particularly focus on RSRP, MCS, BLER, and throughput and discuss their behavior in response to the mobility scenario.

Before applying the time variations of the channel induced by the mobility scenario, we performed a baseline measurement as a reference with the same experimental setup as shown on the right side of Fig. 1 without applying any CIR. This means that, in the baseline measurement, $|s| = |\bar{h}| = 1$ in (4). The 100-second average values of KPIs are summarized in Table 4.

Figs. 6 and 7 summarize the time evolutions of various KPIs output by OAI during the execution of the Shin-nakano and Shibuya scenarios, respectively. The bands shown in lighter shades of the same color as each plot represent the upper and lower bounds observed when the corresponding scenario was executed ten times, indicating the range of error margins.

For the CIR data generated in the previous section, the value of s^2 was configured so that (5-[the maximum path gain within the scenario]) dB was achieved in (4) to maintain a stable connection without interruptions in KPI measurements throughout the scenario. Additionally, since noise power was not the primary focus of this study, σ^2 was set to -100 dBm. Therefore, it should be noted that the absolute values of the observed RSRP in this study are not necessarily realistic, and the emphasis is placed on relative changes in RSRP throughout the scenario.

First, the variations in RSRP obtained from OAI and path gain from Sionna RT, as shown in Figs. 6(a) and 7(a), exhibit a generally consistent trend. For example, in both scenarios, a plateau in RSRP is observed during the red traffic light periods in both DL and UL. However, the short-term fluctuations of approximately 20 dB and the long-term variations in the 18-44 second interval in path gain of the Shin-nakano scenario are not fully reflected in the observed RSRP. This discrepancy is likely due to the KPI averaging process performed by the OAI gNB and the automatic gain control (AGC) function that may be implemented in the commercial UE. As a result, particularly in the Shin-nakano scenario, a level adjustment of approximately 20-30 dB might have occurred within the aforementioned time interval.

Furthermore, the lower sections of these figures show that MCS, BLER, and throughput fluctuate in response to the time variations in RSRP. Here, we quantitatively examine

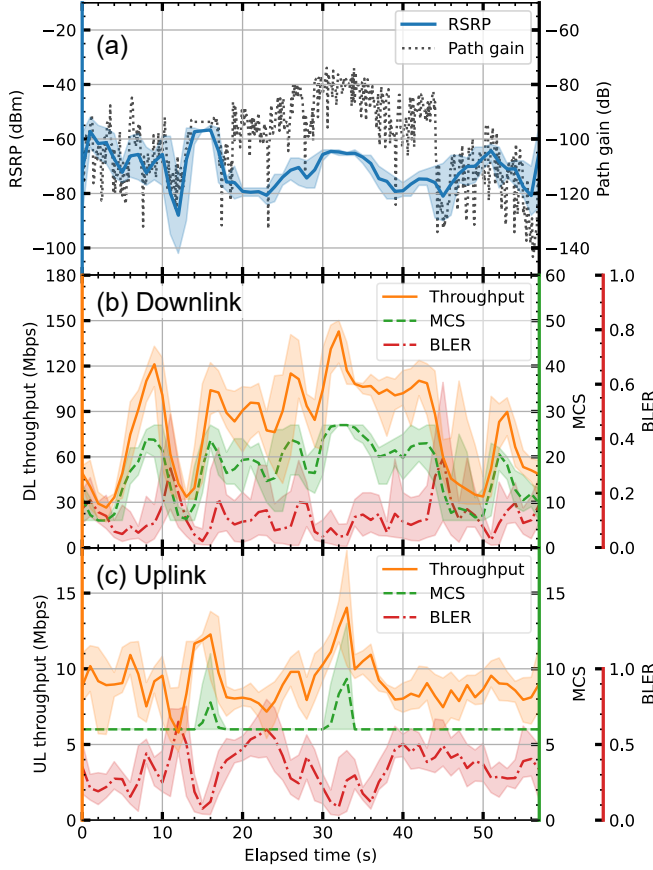


FIGURE 6. (a) RSRP with path gain obtained from RT simulation as a reference, (b) DL KPIs, and (c) UL KPIs obtained from OAI for Shin-nakano scenario.

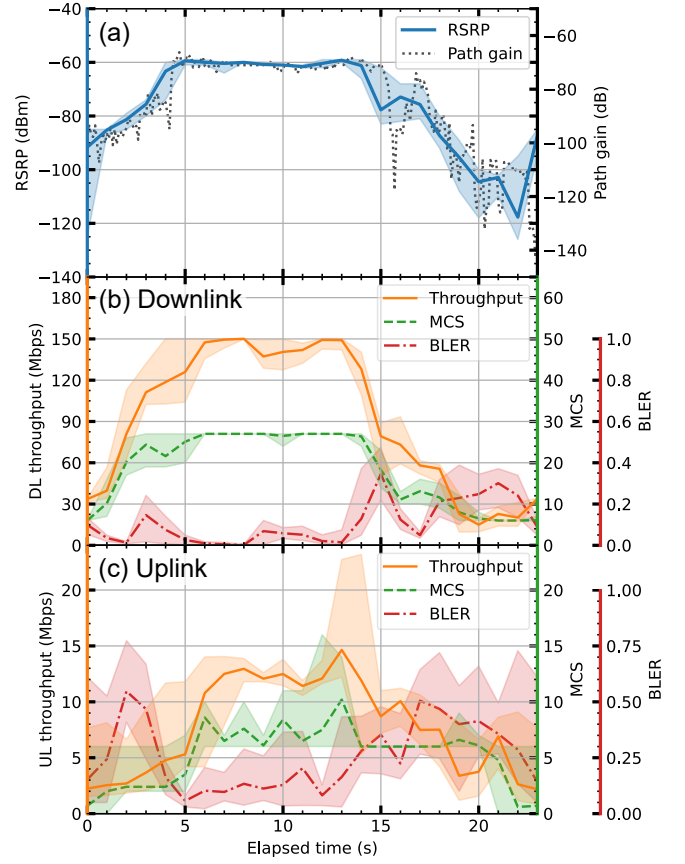


FIGURE 7. (a) RSRP with path gain obtained from RT simulation as a reference, (b) DL KPIs, and (c) UL KPIs obtained from OAI for Shibuya scenario.

the throughput values. The maximum bitrate R_b [Mbps] of 5G NR can be estimated using the following formula, as specified in 3GPP TS 38.306 [44]:

$$R_b = 10^{-6} Q_m R_{\max} \frac{12 N_{\text{PRB}}^{BW}}{T_{\text{symb}}} (1 - OH) \quad (5)$$

$$= \begin{cases} 30.62976 \eta & (\text{for DL}) \\ 32.76672 \eta & (\text{for UL}). \end{cases} \quad (6)$$

Note that the notation is simplified by assuming the number of MIMO layers as 1, the number of aggregated component carriers as 1, and the scaling factor as 1. Here, the modulation order Q_m and the coding rate R_{\max} , and their product, the spectral efficiency η are uniquely determined by the MCS index in TS 38.214 Table 5.1.3.1-2 [45], respectively. N_{PRB}^{BW} represents the number of physical resource blocks (PRBs) within BW , determined by the frequency range and numerology. T_{symb} is the average OFDM symbol duration in a subframe, and OH represents the control channel overhead. Some variables are determined by the parameters in Table 3 and remain unchanged throughout the scenario as $N_{\text{PRB}}^{BW} = 106$, $T_{\text{symb}} = 3.57$ [μs], and OH is 0.14 for DL and 0.08 for UL. By substituting these specific values, the resulting equation is given in (6). The effective throughput

for DL (UL) $T_{\text{DL(UL)}}^{\text{eff}}$ is defined as the actual received data rate, which is given in the case of TDD mode by:

$$T_{\text{DL(UL)}}^{\text{eff}} = (1 - BLER) \alpha_{\text{DL(UL)}} R_b, \quad (7)$$

where $BLER$ represents the block error rate defined by the ratio of the number of erroneous blocks to the total number of transmitted blocks and $\alpha_{\text{DL(UL)}}$ indicates the time occupancy ratio of DL (UL) determined by the TDD slot pattern and special slot format. In the case of the TDD pattern shown in Table 3, the DL ratio is given by $\alpha_{\text{DL}} = 0.6857$, while the UL ratio is given by $\alpha_{\text{UL}} = 0.2571$, and thus, $T_{\text{DL(UL)}}^{\text{eff}}$ can be expressed as follows:

$$T_{\text{DL}}^{\text{eff}} = 21.003264 (1 - BLER) \eta \quad (8)$$

$$T_{\text{UL}}^{\text{eff}} = 8.425728 (1 - BLER) \eta. \quad (9)$$

Therefore, it can be concluded that the effective throughput can be calculated based on the spectral efficiency η corresponding to the MCS index and $BLER$. Accordingly, we focus on the variations in MCS and $BLER$ depending on the mobility scenario. In the two scenarios analyzed, the maximum observed DL throughput was 150.0778 Mbps. At this point, the MCS = 27 and $BLER = 0.001656$. Using (8), the calculated effective throughput is 155.2989 Mbps, showing a close match between measurement and

calculation. On the other hand, the maximum observed UL throughput was 14.64214 Mbps. At this point, the MCS = 10, and the $BLER = 0.163917$. Using (9), the calculated effective throughput is 18.106756 Mbps. The discrepancy in UL throughput compared to the DL throughput can be attributed to, for example, the presence of sounding reference signals (SRSs) which occupy a portion of PRBs in UL transmission. Therefore, the KPIs measured by KPM xApps can be considered consistent with theoretical expectations. Measured throughputs show maximum when the UE comes closest to the gNB, BLER exhibits an inverse trend to throughput, and MCS changes in near-proportional relation to throughput, indicating highly reasonable results. When comparing Figs. 6(b) and (c), examining the difference between DL and UL, it becomes apparent that UL variations are not as pronounced as those in DL. BLER is significantly higher, and to maintain UL communication quality, MCS is automatically set lower to limit the modulation order, resulting in lower UL throughput. Potential causes of errors include: (i) modulation and demodulation methods, (ii) modulation symbol period, (iii) characteristics of bandwidth limitation filters, (iv) channel characteristics, and (v) timing offsets due to cycle slips. These errors originate from both system factors and radio propagation. If we focus solely on propagation aspects, the relevant factors are (iv) and (v). Since this study does not consider the vehicle's velocity vector, the possibility of cycle slips caused by fast fading is eliminated. Consequently, inter-symbol interference (ISI) errors caused by multipath propagation with varying arrival times remain the primary concern. The Cyclic Prefix (CP) in CP-OFDM, used in 5G NR, is a technique designed to mitigate ISI. In our communication system parameters, the long CP assigned to the first OFDM symbol contains 132 samples corresponding to 2.86 μs , while subsequent short CPs contain 106 samples corresponding to 2.30 μs . If, within the 146 CIR taps used in this study, significant complex amplitudes are found in taps exceeding 132 samples, throughput could be affected. In our environment, the real-time processing limit was $L_{\text{OAI}} = 28$ taps, and no delay tap index exceeding 2.30 μs was observed. Thus, it is concluded that ISI due to multipath propagation is not an issue in these scenarios and the error observed in UL is considered to originate from the system. In fact, as seen in Table 4, the UL BLER was already close to 10% during the baseline measurement, which may be related to the implementation of the received signal processing on the gNB side.

C. FUTURE PROSPECTS

When discussing future intelligent transportation systems, it is necessary to consider methods for appropriately evaluating mobility scenarios where the statistical properties of channels change rapidly over time in dynamic radio environments. While ray tracing achieves high-resolution results in static channel modeling, it becomes significantly more complex in dynamic scenarios involving high-speed

moving vehicles, where the wide-sense-stationarity (WSS) assumption is violated. Generally, for mobile entities in multipath environments, both frequency-selective fading and time-selective fading must be considered as doubly selective fading. However, realistically incorporating the effects of both types of fading into baseband signal processing and executing real-time E2E wireless communication is extremely challenging due to computational load. To address this challenge, we aim to explore real-time processing using acceleration technologies such as FPGAs and GPUs in future work.

Furthermore, a key feature of this study is that all workflows and system architectures are built entirely using OSS and open data. However, each OSS component has its own limitations and constraints. The OWDT architecture we constructed serves as a reference architecture, and each component can be substituted with any proprietary products or alternative OSS implementations. The CIR convolution implementation for OAI developed in this study, along with sample scenarios, will be contributed as OAI source code and made publicly available as OSS wherever possible.

Future challenges include support for the representation of Doppler effects. In higher frequency bands such as FR2, Doppler shift affects communication quality, so its impact needs to be implemented in detail. To simulate MIMO spatial multiplexing transmission as well as beamforming for high-frequency bands on OWDT, it is essential to incorporate multi-antenna ray tracing. This is particularly crucial for Massive MIMO, where a gNB is equipped with a large-scale antenna array. A key challenge lies in efficiently and in real-time generating a large number of propagation paths. Beamforming also necessitates tracking moving targets that may lead to frequent handovers. If OWDT can accurately represent this, it would enable the development of a solution for managing handovers across the entire system. To achieve these objectives, the following extensions are also required: integration with higher-precision 3D models and mobility scenarios, scalability in terms of the number of gNBs and UEs, utilization of acceleration technologies such as GPUs and FPGAs to enable real-time processing, and validation through comparison with experimental data to establish a truly representative digital twin.

IV. CONCLUSION

This study proposed the OWDT, an E2E 5G mobility emulation framework that can be deployed as the O-RAN ecosystem. By combining OAI for protocol stack emulation and Sionna RT for ray tracing based RF modeling, OWDT enables high-fidelity performance evaluation in vehicular mobility scenarios. To achieve real-time emulation, we implemented a convolution method that applies precomputed time-evolving CIRs to baseband IQ signals. This method efficiently reproduces multipath fading effects while ensuring real-time processing within the constraints of COTS hardware. The framework leverages Near-RT RIC via FlexRIC

to monitor key performance indicators (KPIs) such as RSRP, MCS, BLER, and throughput, providing real-time insights into wireless communication system behavior. Experimental validation demonstrated that OWDT effectively replicates real-world channel conditions, supporting efficient network performance analysis and optimization with minimal physical deployment. This approach significantly reduces the cost and accelerates the development of wireless communication systems. Future work will focus on Doppler effects, FR2/beamforming, and scalability with multi-UE/gNB configurations to enhance emulation fidelity and usability.

ACKNOWLEDGMENT

We would like to thank Luis Pereira and Paulo Marques from Allbesmart LDA for the fruitful discussion on the OAI implementation.

The authors used generative AI tools such as ChatGPT and Grammarly to improve the grammar of the manuscript. After using these tools, they carefully reviewed and edited the content and took full responsibility for the published manuscript.

REFERENCES

- [1] F. A. Butt, J. N. Chattha, J. Ahmad, M. U. Zia, M. Rizwan, and I. H. Naqvi, "On the integration of enabling wireless technologies and sensor fusion for next-generation connected and autonomous vehicles," *IEEE Access*, vol. 10, pp. 14 643–14 668, 2022.
- [2] Y. Asabe, E. Javanmardi, J. Nakazato, M. Tsukada, and H. Esaki, "Enhancing reliability in infrastructure-based collective perception: A dual-channel hybrid delivery approach with real-time monitoring," *IEEE Open Journal of Vehicular Technology*, vol. 5, pp. 1124–1138, 2024.
- [3] L. U. Khan, Z. Han, W. Saad, E. Hossain, M. Guizani, and C. S. Hong, "Digital twin of wireless systems: Overview, taxonomy, challenges, and opportunities," *IEEE Communications Surveys & Tutorials*, vol. 24, no. 4, pp. 2230–2254, 2022.
- [4] S. Furuta, J. Nakazato, and M. Tsukada, "Web-based bim platform for building digital twin," in *2023 IEEE 3rd International Conference on Digital Twins and Parallel Intelligence (DTPi)*, 2023, pp. 1–6.
- [5] F. Kojima, T. Miyachi, T. Matsumura, H. Sawada, H. Harai, and H. Harada, "A large-scale wireless emulation environment with interaction between physical and virtual radio nodes for beyond 5g systems," in *2022 IEEE 33rd Annual International Symposium on Personal, Indoor and Mobile Radio Communications (PIMRC)*, 2022, pp. 1–6.
- [6] T. Matsumura, H. Sawada, T. Miyachi, F. Kojima, H. Harai, A. Sakaguchi, Y. Nishigori, and H. Harada, "Development and initial implementation of large-scale wireless emulator toward beyond 5g," in *2022 25th International Symposium on Wireless Personal Multimedia Communications (WPMC)*, 2022, pp. 199–204.
- [7] S. Mori, K. Mizutani, and H. Harada, "Software-defined radio-based 5g physical layer experimental platform for highly mobile environments," *IEEE Open Journal of Vehicular Technology*, vol. 4, pp. 230–240, 2023.
- [8] M. Polese, L. Bonati, S. D'Oro, P. Johari, D. Villa, S. Velumani, R. Gangula, M. Tsampazi, C. P. Robinson, G. Gemmi, A. Lacava, S. Maxenti, H. Cheng, and T. Melodia, "Colosseum: The open ran digital twin," 2024. [Online]. Available: <https://arxiv.org/abs/2404.17317>
- [9] P. Testolina, M. Polese, P. Johari, and T. Melodia, "Boston twin: the boston digital twin for ray-tracing in 6g networks," in *Proceedings of the 15th ACM Multimedia Systems Conference*, ser. MMSys '24. New York, NY, USA: Association for Computing Machinery, 2024, p. 441–447. [Online]. Available: <https://doi.org/10.1145/3625468.3652190>
- [10] D. Villa, I. Khan, F. Kalteneberger, N. Hedberg, R. S. Da Silva, A. Kelkar, C. Dick, S. Basagni, J. M. Jornet, T. Melodia, M. Polese, and D. Koutsonikolas, "An open, programmable, multi-vendor 5g o-ran testbed with nvidia arc and openairinterface," in *IEEE INFOCOM 2024 - IEEE Conference on Computer Communications Workshops (INFOCOM WKSHPS)*, 2024, pp. 1–6.
- [11] S. Jiang, Q. Qu, X. Pan, A. Agrawal, R. Newcombe, and A. Alkhateeb, "Learnable wireless digital twins: Reconstructing electromagnetic field with neural representations," 2024. [Online]. Available: <https://arxiv.org/abs/2409.02564>
- [12] D. Radovic, M. Hofer, F. Pasic, E. M. Vitucci, A. Fedorov, and T. Zemen, "Methodologies for future vehicular digital twins," 2023. [Online]. Available: <https://arxiv.org/abs/2312.09902>
- [13] J. Nakazato, T. Iye, Y. Susukida, E. Sato, Y. Sasaki, K. Maruta, and M. Tsukada, "Toward 6g mobility network: Design of a wireless digital twin for connected autonomous vehicle," 2025 IEEE 22nd Consumer Communications & Networking Conference (CCNC), Poster, pp. 1–2, 2025.
- [14] R. Pegurri, F. Linsalata, E. Moro, J. Hoydis, and U. Spagnolini, "Toward digital network twins: Integrating sionna rt in ns-3 for 6g multi-rat networks simulations," 2025. [Online]. Available: <https://arxiv.org/abs/2501.00372>
- [15] F. Kalteneberger, A. P. Silva, A. Gosain, L. Wang, and T.-T. Nguyen, "Openairinterface: Democratizing innovation in the 5g era," *Computer Networks*, vol. 176, p. 107284, 2020. [Online]. Available: <https://www.sciencedirect.com/science/article/pii/S1389128619314410>
- [16] free5GC.org, "free5GC." [Online]. Available: <https://free5gc.org/>
- [17] "Open5GS." [Online]. Available: <https://open5gs.org/>
- [18] Magma Core Foundation, "Magma." [Online]. Available: <https://magmacore.org/>
- [19] AETHER, "AETHER Project." [Online]. Available: <https://aetherproject.org/>
- [20] Software Radio Systems, "srsRAN." [Online]. Available: <https://www.srslte.com/>
- [21] "UERANSIM." [Online]. Available: <https://github.com/aligungr/UERANSIM>
- [22] J. Hoydis, S. Cammerer, F. A. Aoudia, A. Vem, N. Binder, G. Marcus, and A. Keller, "Sionna: An open-source library for next-generation physical layer research," 2023. [Online]. Available: <https://arxiv.org/abs/2203.11854>
- [23] Accelleran, "dRAX." [Online]. Available: <https://github.com/aligungr/UERANSIM>
- [24] O-RAN Software Community. [Online]. Available: <https://o-ran-sc.org/>
- [25] J. Hoydis, F. A. Aoudia, S. Cammerer, M. Nimier-David, N. Binder, G. Marcus, and A. Keller, "Sionna rt: Differentiable ray tracing for radio propagation modeling," 2023. [Online]. Available: <https://arxiv.org/abs/2303.11103>
- [26] Ericsson, "Network digital twins - outlook and opportunities." [Online]. Available: <https://www.ericsson.com/en/reports-and-papers/ericsson-technology-review/articles/network-digital-twins-outlook-and-opportunities>
- [27] E2 Service Model (E2SM), KPM. Technical Specification O-RAN.WG3.E2SM-KPM-R003-v03.00. O-RAN Working Group 3., "O-RAN E2 Service Model (E2SM) KPM 3.0," 2023.
- [28] R. Schmidt, M. Irazabal, and N. Nikaein, "Flexric: an sdk for next-generation sd-rans," in *Proceedings of the 17th International Conference on Emerging Networking EXperiments and Technologies*, ser. CoNEXT '21. New York, NY, USA: Association for Computing Machinery, 2021, p. 411–425. [Online]. Available: <https://doi.org/10.1145/3485983.3494870>
- [29] Ministry of Land, Infrastructure, Transport and Tourism, "Project plateau." [Online]. Available: <https://www.mlit.go.jp/plateau/>
- [30] OpenStreetMap contributors, "Planet dump retrieved from <https://planet.osm.org>," <https://www.openstreetmap.org>, 2017.
- [31] Blender Online Community, *Blender - a 3D modelling and rendering package*, Blender Foundation, Stichting Blender Foundation, Amsterdam, 2018. [Online]. Available: <http://www.blender.org>
- [32] Blender-OSM, "Openstreetmap and terrain for blender." [Online]. Available: <https://prochitecture.gumroad.com/blender-osm>
- [33] Mitsuba Blender Add-on. [Online]. Available: <https://github.com/mitsuba-renderer/mitsuba-blender>
- [34] ITU-R, "Effects of building materials and structures on radiowave propagation above about 100 mhz," pp. 2040–2.

- [35] P. A. Lopez, M. Behrlich, L. Bieker-Walz, J. Erdmann, Y.-P. Flötteröd, R. Hilbrich, L. Lücken, J. Rummel, P. Wagner, and E. Wiebner, "Microscopic traffic simulation using sumo," in *2018 21st International Conference on Intelligent Transportation Systems (ITSC)*. IEEE Press, 2018, p. 2575–2582. [Online]. Available: <https://doi.org/10.1109/ITSC.2018.8569938>
- [36] Remcom, "Wireless insite." [Online]. Available: <https://www.remcom.com/wireless-insite-propagation-software>
- [37] E. Egea-Lopez, J. M. Molina-Garcia-Pardo, M. Lienard, and P. Degauque, "Opal: An open source ray-tracing propagation simulator for electromagnetic characterization," *PLOS ONE*, vol. 16, no. 11, pp. 1–19, 11 2021. [Online]. Available: <https://doi.org/10.1371/journal.pone.0260060>
- [38] Altair, "Winprop." [Online]. Available: <https://altair.com/>
- [39] MathWorks, "Raytracing." [Online]. Available: <https://mathworks.com/help/antenna/ref/rfprop.raytracing.html>
- [40] H. Choi, J. Oh, J. Chung, G. C. Alexandropoulos, and J. Choi, "Withray: A versatile ray-tracing simulator for smart wireless environments," *IEEE Access*, vol. 11, pp. 56 822–56 845, 2023.
- [41] BLIS, "BLIS." [Online]. Available: <https://github.com/flame/blis>
- [42] Y. Karasawa, "On physical limit of wireless digital transmission from radio wave propagation perspective," *Radio Science*, vol. 51, no. 9, pp. 1600–1612, 2016. [Online]. Available: <https://agupubs.onlinelibrary.wiley.com/doi/abs/10.1002/2016RS006040>
- [43] M. Hofer, Z. Xu, D. Vlastaras, B. Schrenk, D. Löschenbrand, F. Tufvesson, and T. Zemen, "Real-time geometry-based wireless channel emulation," *IEEE Transactions on Vehicular Technology*, vol. 68, no. 2, pp. 1631–1645, 2019.
- [44] 3GPP TS 38.306: "NR; User Equipment (UE) radio access capabilities".
- [45] 3GPP TS 38.214: "NR; Physical layer procedures for data".



TETSUYA IYE received the B.S. degree in physics from Waseda University, Tokyo, Japan, in 2009 and the M.S. and Ph.D. degrees in physics from Kyoto University, Kyoto, Japan, in 2011 and 2014, respectively. From 2013 to 2014, he was a Research Fellow of the Japan Society for the Promotion of Science. He joined Kozo Keikaku Engineering Inc., Tokyo, Japan, as a System Engineer in 2014. After gaining experience in developing CAD-related systems, vibration analysis, IoT system development, and machine learning, he

has been engaged in research and development of next-generation mobile communication systems since 2019. His research interests include software-defined radio, antennas and propagation, beamforming, signal processing, mathematical optimization, deep learning, quantum computing, and large language models.



MASAYA SAKAMOTO received the B.S. in physics from Tokyo Metropolitan University, Tokyo, Japan, in 2024. In the same year, he began collaborative work with the Communication Engineering Department at Kozo Keikaku Engineering Inc., Tokyo, Japan, as an independent research engineer specializing in data analysis and algorithm design. His research interests include deep learning and the geometric properties of its hidden layers.



SHOHEI TAKAYA received the B.E. degree in electrical and electronic engineering from Tokyo Denki University, Japan, in 2016. From 2016 to 2020, he worked at Miraxia Edge Technology Corporation. Since 2021, he has been working at Kozo Keikaku Engineering Inc.. He is engaged in research and development of 5G systems and radio propagation emulation using software-defined radios (SDR). He is a member of IEICE.



EISAKU SATO Eisaku Sato received the B.E. and M.E. degrees from Toyohashi University of Technology, Japan, in 2021 and 2023, respectively. In 2023, he joined Kozo Keikaku Engineering Inc., Japan, as a wireless communication engineer. His current research and development interests include system-level simulations and wireless signal processing. He is a member of IEICE.



YUKI SUSUKIDA received his B.S. and M.S. degrees in Seismology from Hokkaido University, Japan, in 2020. Since 2020, he has been working at Kozo Keikaku Engineering Inc., focusing on the research and development of wireless access systems using software-defined radio technologies. Recently, his work has involved the development of wireless access systems utilizing OpenAirInterface, an open-source software platform for 5G communication systems. His research interests include 5G V2X, 5G NTN, and Integrated Sensing and Communication (ISAC).



YU NAGAOKA received the B.E. degree in Electronics and Computer Systems from Takushoku University, Japan, in 2024. Since 2024, he has been pursuing the M.E. degree in Mechanical and Electronic Systems Engineering at the Graduate School of Engineering, Takushoku University. His current research interests include wireless communication systems and communication protocols. He is a member of IEICE.



KAZUKI MARUTA (Senior Member, IEEE) received the B.E., M.E., and Ph.D. degrees in engineering from Kyushu University, Japan in 2006, 2008 and 2016, respectively. From 2008 to 2017, he was with NTT Access Network Service Systems Laboratories. From 2017 to 2020, he was an Assistant Professor at the Graduate School of Engineering, Chiba University. From 2020 to 2022, he was a specially appointed Associate Professor at the Academy for Super Smart Society, Tokyo Institute of Technology. He is currently an Associate

Professor at the Department of Electrical Engineering, Tokyo University of Science. His research interests include MIMO, massive MIMO, adaptive array signal processing, channel estimation, moving networks, visible light communication, and underwater acoustic communication. He is a senior member of IEEE and IEICE. He serves as a Poster Co-Chair for IEEE CCNC from 2023 to 2025. He received the IEICE Young Researcher's Award in 2012, the IEICE Radio Communication Systems Active Researcher Award in 2014, APMC2014 Prize, the IEICE RCS Outstanding Researcher Award in 2018, the IEEE ICCE Excellent Paper Award in 2021, and ICAIC 2024 Excellent Paper Award. He was a co-recipient of the IEICE Best Paper

Award in 2018, APCC 2019 Best Paper Award, and ICCE-Asia 2022 Best Paper Award.



JIN NAKAZATO (Member, IEEE) is currently a specially appointed Assistant Professor at the University of Tokyo. He also works as a technical advisor with Visban Corporation. He received B.E. and M.E. degrees from the University of Electro-Communications, Japan, in 2014 and 2016, respectively. He received a Ph.D. degree from the Tokyo Institute of Technology, Japan, in 2022. From 2016 to 2020, he was with Fujitsu Limited. From 2020 to 2022, he was with Rakuten Mobile, Inc. His research interests include Multi-access

Edge Computing, NFV/SDN Orchestrator, V2X, Open RAN, UAV networks, and virtualization RAN. He is a Member of IEICE, IEEE, and WIDE Project. He received the Best Paper Award at the International Conference on Ubiquitous and Future Networks (ICUFN) in 2019 and 2024, respectively. He also received the Best Paper Award at the INFOCOM 2024, ICAIIC Excellent Paper Award, and ACM ICEA Best Paper Award. He serves as an editor of IEICE Communications Express (ComEX), a peer-reviewed open-access letter journal covering the field of communication, and the International Journal of Computers Applications Associate Editor.